Serrano, A., Rubio-Zuazo, J., López-Sánchez, J., Enríquez, E., Salas-Colera, E., & Castro, G. R. (2019). Nanostructured AU(111)/oxide epitaxial heterostructures with tailoring plasmonic response by a one-step strategy. *Journal of Physical Chemistry C*, 123(41), 25294-25302.

DOI: 10.1021/acs.jpcc.9b04768

THE JOURNAL OF PHYSICAL CHEMISTRY C

Article

pubs.acs.org/JPCC

Nanostructured Au(111)/Oxide Epitaxial Heterostructures with Tailoring Plasmonic Response by a One-Step Strategy

Aida Serrano,[*,†,‡] Juan Rubio-Zuazo,[†,‡] Jesús López-Sánchez,[§,∥] Esther Enríquez,[⊥,#] Eduardo Salas-Cólera,[†,‡] and Germán R. Castro[†,‡]

[†]Spanish CRG BM25-SpLine at The ESRF—The European Synchrotron, 38000 Grenoble, France

[‡]Instituto de Ciencia de Materiales de Madrid (ICMM), CSIC, 28049 Madrid, Spain

[§]Departamento de Física de Materiales, Universidad Complutense de Madrid, 28040 Madrid, Spain

[∥]Instituto de Magnetismo Aplicado (UCM-CSIC-ADIF), 28230 Madrid, Spain

[⊥]Instituto de Cerámica y Vidrio (ICV), CSIC, 28049 Madrid, Spain

[#]Centro tecnológico Vidres, S.L. Ctra. Onda, Km 3.4, 12540 Villareal, Castellon, Spain

Supporting Information

ABSTRACT: In this work, we present a strategy for developing epitaxial incommensurate nanostructured Au/oxide heterostructures with tunable plasmonic response. Previously, high-quality single-phase and single-oriented α-Fe_2O_3(0001) thin films were achieved, which have been used as a template for noble-metal epitaxial deposition. The complex systems have been grown by pulsed laser deposition on two different types of oxide substrates: α-Al_2O_3(0001) and $SrTiO_3$(111). A one-step procedure has been achieved tailoring the isolated character and the morphological features of Au nanostructures through the substrate temperature during Au growth, without altering the structural characteristics of the hematite layer that is identified as a single iron oxide phase. The epitaxial character and the lattice coupling of Au/oxide bilayers are mediated through the sort of oxide substrate. Single-oriented Au(111) islands are disposed with a rotation of 30° between their crystallographic axes and those of α-Fe_2O_3(0001). The Au(111) and $SrTiO_3$(111) lattices are collinear, while a rotation of 30° happens with respect to the α-Al_2O_3(0001) lattice. The crystallographic domain size and crystalline order of the hematite structure and the Au nanostructured layer are dependent on the substrate type and the Au growth temperature, respectively. Besides, the functional character of the complex systems has been tested. The localized surface plasmons related to Au nanostructures are excited and controlled through the fabrication parameters, tuning the optical resonance with the degree of Au nanostructuring.

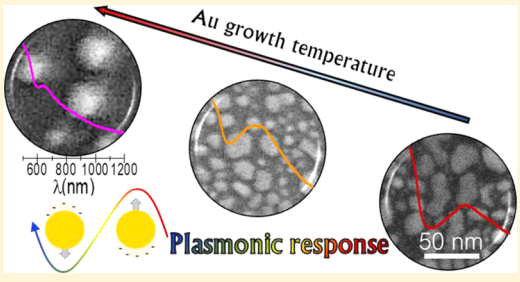

1. INTRODUCTION

Hybrid nanomaterials receive a great attention from both fundamental and applied points of view due mainly to coupling effects and enhanced properties over the single components.[1−6] In this aspect, these materials in which one of the constituents is based on noble metals exhibiting surface plasmon resonance (SPR) response suppose an excellent system for active applications as the heterogeneous catalysis.[1,2,5,7,8] For example, noble nanoparticles (NPs) supported on iron oxides are highly attractive to improve the catalytic activity.[1,2,9] Besides, the surface of epitaxial iron oxide films has been shown as an appealing framework to support the noble-metal nanostructures (NSs) exhibiting a large rate of oxidation.[10−12] Specifically, α-Fe_2O_3 (hematite) is one of the iron oxides with a high potential for numerous applications due to its richness, nontoxic nature, and high chemical stability. This iron oxide polymorph has already been proposed as an active oxide for CO oxidation at low temperature and for water splitting processes.[13,14] In addition, a great photochemical reactivity for the Ag reduction has been proven in the specific configuration of the epitaxial α-Fe_2O_3 film prepared on $SrTiO_3$(111).[15]

Au NSs have been extensively studied in a wide range of investigation areas such as catalysis, magnetism, or plasmonics.[16−19] Specially, integrated or supported Au NPs are quite acclaimed due to their active response presenting SPR to functionalize materials.[1−3,9,20−22] The final response of noble-metal NSs is dependent on morphological and structural parameters such as the geometry, the crystallinity, or the surrounding media among others, favoring to control the final properties with the growth conditions and so tailoring the implications in each field.

An interesting method to change in a controlled way the morphological features of noble metallic NSs on oxide surfaces is the well-known dewetting process.[23,24] Dewetting of metallic thin films can be achieved in several ways. The most employed

Received: May 20, 2019
Revised: September 23, 2019
Published: September 24, 2019

DOI: 10.1021/acs.jpcc.9b04768
J. Phys. Chem. C XXXX, XXX, XXX−XXX

method to achieve a nanostructured character from an initial continuous film is by means of a *posteriori* thermal treatment at a defined temperature.[19,25] Other methodologies to induce the dewetting mechanism can be by the irradiation with an electron or ion beam on the desired region[26,27] or by using a prestructured template on which the film is submitted to the dewetting process.[28] Other method much less widespread but advantageous consists in the dewetting process during the film growth retaining the heterostructure up to a certain temperature and so avoiding a subsequent annealing process after the film deposition.[10,29] In this way, the control of the resulting morphology of NSs is also possible tuning accurately the growth parameters. During the growth process in which the substrate is maintained at a specific temperature, the mobility of the metallic atoms on the surface is really large enhancing the superficial diffusion process and achieving a stage of three-dimensional (3D) islands. In this sense, the nanostructuration can be tailored with the substrate temperature.

In the present work, epitaxial Au(111) NPs are formed on oxide heterostructures (α-Fe_2O_3 layer/oxide substrate) by a one-step strategy in which the control of the morphological and structural parameters is performed through the substrate temperature during the Au growth by subsequent deposition, i.e., without breaking the vacuum in the growth chamber and without a *posteriori* post-treatment of samples. The effect of the underlying substrate is evaluated by using two different oxide substrates, which induces different macroscopic behavior on the oxide heterostructure surface. Besides, we discuss the ability of the growth process to achieve the Au nanostructuration without alteration of the iron oxide properties and tuning the plasmonic activity of complex system.

Based on a previous work,[30] we use high-quality single-phase and single-oriented α-Fe_2O_3(0001) thin films grown on $SrTiO_3$ (STO)(111) and α-Al_2O_3 (AO)(0001) oxide substrates as a bare template for the Au NPs deposition. The identification of the lattice coupling mechanism and the morphological and structural characteristics of the hematite layers as a function of lattice parameter and crystallographic orientation of substrate were studied in such a work.[30] We concluded that high-quality epitaxial hematite layers with bulklike structure and free of oxygen vacancies defects were obtained on both substrates. However, although the hematite layers behaved identical on both oxide substrates in terms of microscopic roughness and interface abruptness, the macroscopic surface and interface quality of the hematite layers were different as revealed by the presence and absence of Kiessig fringes in the X-ray reflectivity (XRR), specular and off-specular X-ray diffraction (XRD) patterns. Such a difference may induce important modifications on the nanostructuration process of the Au. Hence, the achieved α-Fe_2O_3(0001)/STO(111) and α-Fe_2O_3(0001)/AO(0001) systems become ideal candidates as templates for the study of the formation and morphological tuning of Au NPs on oxide heterostructures.

2. EXPERIMENTAL METHODS

Epitaxial Au NPs were grown by pulsed laser deposition (PLD) on α-Fe_2O_3(0001)/AO(0001) and α-Fe_2O_3(0001)/STO(111) oxide heterostructures. The growth was performed by using an ultraviolet (UV) pulsed laser source (355 nm) of high power (1 W) to obtain the plasma and a base pressure of 10^{-9} mbar. Previously, continuous and homogeneous iron oxide (hematite) films were deposited by PLD under an O_2 atmosphere (P_{O_2} of 10^{-4} mbar) with the AO(0001) and STO(111) substrates at 400 °C using an α-Fe_2O_3 target, following the same procedure as that in our previous work.[30] Subsequently, nanostructured Au layers were grown on hematite layers from a Au target keeping the oxygen pressure P_{O_2} about 10^{-4} mbar at three different substrate temperatures: 250, 500, and 750 °C. Deposition dose (mass thickness) was fixed for iron oxide and Au, respectively. During the deposition process, the crystalline character of both layers was confirmed by in situ reflection high-energy electron diffraction obtaining intense patterns from the initial stages of deposition, as shown in the Supporting Information (SI). Table 1 shows the set of samples selected for this work.

Table 1. Representative Nanostructured Au/α-Fe_2O_3/oxide Substrate Systems Selected for this Work, in Which the Type of Substrate and the Substrate Temperature for the Au Growth are Varied

sample	substrate	Au growth temperature (°C)
AO_250	AO(0001)	250
AO_500	AO(0001)	500
AO_750	AO(0001)	750
STO_250	STO(111)	250
STO_500	STO(111)	500
STO_750	STO(111)	750

The morphology of the Au NPs on oxide heterostructures was studied by scanning electron microscopy (SEM) with an S-4700 Hitachi instrument at 20 kV, and the morphological features were examined by using ImageJ software. Grazing incidence X-ray diffraction (GIXRD), XRR, and X-ray absorption spectroscopy (XAS) were carried out at the Spanish CRG synchrotron beamline BM25-SpLine at The ESRF—The European Synchrotron, Grenoble (France). GIXRD and XRR measurements were carried out in a high-precision six-circle diffractometer in vertical geometry[31] at room temperature (RT) using a photon wavelength of 0.826 Å ($h\nu$ = 15 keV). XAS measurements were performed at the Fe K-edge (7112 eV) and the Au L_3-edge (11919 eV) at RT in fluorescence detection mode using a 13-element Si(Li) detector located 90° with respect to the incoming X-ray beam. Spectra of reference standards (Au foil, Fe foil, FeO, Fe_3O_4, α-Fe_2O_3, and γ-Fe_2O_3) were collected for comparison in transmission detection mode with two ionization chambers as detectors. XAS data were analyzed using the Demeter package.[32] Optical absorption measurements were collected in transmission mode with an UV−vis−NIR Shimadzu 3100 double-beam spectrophotometer equipped with an integrating sphere. Spectra were recorded at RT from 400 to 1400 nm with a spectral resolution of 0.5 nm.

3. RESULTS AND DISCUSSION

3.1. Morphological and Structural Characterization: Au Nanostructuration. The growth of noble-metal thin films on oxide surfaces is associated with a behavior in which the film deposition proceeds through the nucleation of islands that coalesce resulting in a continuous film. Specifically, 3D islands can be presented directly as a result of the deposition under certain film thickness and specific conditions, being possible to control the final structures.[33,34] Upon annealing, the dewetting mechanism of the metallic film is activated to relieve the

DOI: 10.1021/acs.jpcc.9b04768
J. Phys. Chem. C XXXX, XXX, XXX−XXX

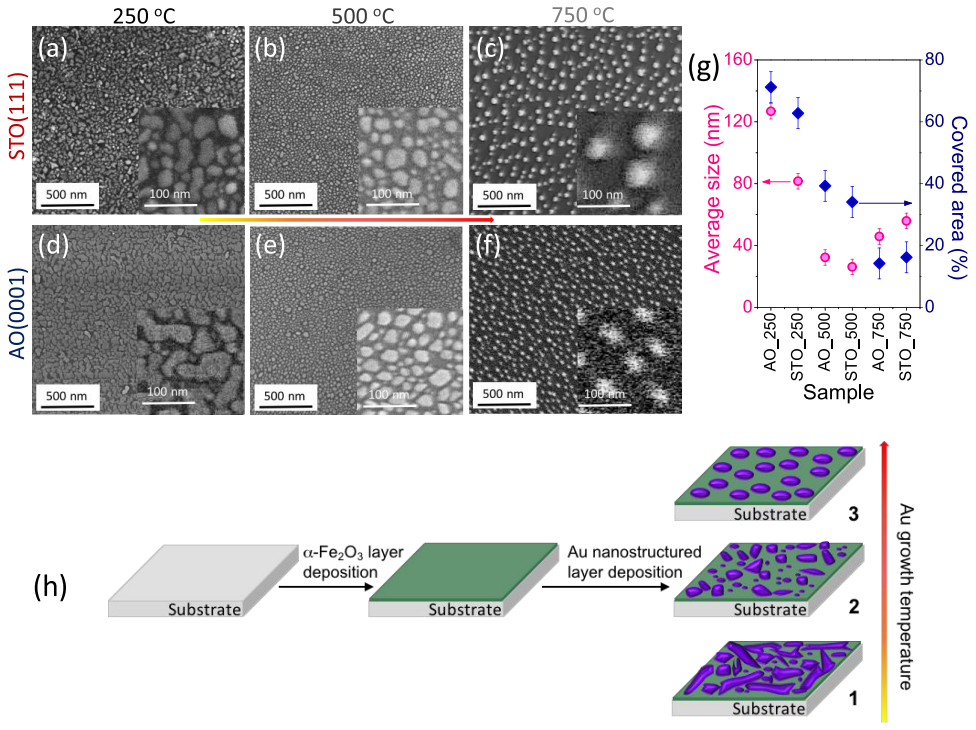

Figure 1. (a–f) SEM images and (g) average size and covered area obtained from SEM images for Au NPs prepared on α-Fe_2O_3(0001)/AO(0001) and α-Fe_2O_3(0001)/STO(111) oxide heterostructures controlling the growth temperature (250, 500, and 750 °C) of the nanostructured Au layer. (h) Representative scheme of growth for the heterostructure system varying the Au growth temperature (1 → 3).

mechanisms of surface and interfacial stress, giving rise to morphological modifications that have been extensively explored.[19,35−37] In this process, the appearance of holes and their subsequent growth is promoted by the surface diffusion, increasing several orders of magnitude in the presence of oxygen, until the holes percolate leading to the formation of islands.[3,23,38,39] In this work, a different procedure is performed in which epitaxial Au nanostructured layers are prepared on hematite surface from high-quality epitaxial thin films (see ref 30) at a certain substrate temperature in just one step.

Figure 1 shows the SEM images for Au NPs prepared on α-Fe_2O_3(0001)/AO(0001) and α-Fe_2O_3(0001)/STO(111) oxide heterostructures varying the substrate temperature in the growth process of the top Au layer. A nanostructured top layer is obtained irrespective of the substrate and its temperature selected for the Au growth. However, a clear evolution of the nanostructured layer features is attained as a function of the substrate temperature: the larger the temperature during the Au growth, the larger is the nanostructuration of layer attaining more rounded and isolated Au NPs. An analysis of the morphological parameters gives values of the covered surface area from 70 to 15%, diminishing as the Au growth temperature increases (see Figure 1g). With respect to the average size of Au NSs, we identify a decrease from around 100 to 30 nm when the Au growth temperature passes from 250 to 500 °C, while for the sample prepared at 750 °C, a slight size increase to around 50 nm is obtained. Specifically, at the highest temperatures, we find more homogeneous Au islands that may be an indication of a more pronounced Oswald's ripening. Besides, seemingly, the morphological effects related to the used substrate and therefore to the characteristics of hematite layers in the final Au islands and their distribution are slight or not presented. Results expected taking into account the slight differences in the values of grain average height and rms roughness of the bare α-Fe_2O_3 films grown on AO(0001) and STO(111) substrates.[30]

Hence, the nanostructuration process of Au layer on α-Fe_2O_3/oxide substrate heterostructures is renowned and the proposed one-step growth procedure provides qualitatively similar morphological results to those in a post-annealing process of a continuous metallic film. A representative scheme of the growth mechanism for nanostructuredA u/α-Fe_2O_3(0001)/oxide substrate system depending on the substrate temperature for the Au growth is represented in Figure 1h. During the Au growth, the Au atoms diffuse as soon as they arrive on the hematite surface because the binding energy between the Au atoms is larger than that between the hematite and Au atoms resulting in Au NSs. Such a nanostructuration is more stable than a continuous thin film. As depicted, the superficial diffusion processes are increased with the substrate temperature during the Au growth, generating a larger Au nanostructuration and islands with certain morphological characteristics (1 → 3).

High-resolution GIXRD and XRR techniques were employed to analyze the substrate effect and the Au growth temperature on the crystallographic character of the system. The layer thickness was calculated from low-angle XRR measurements obtaining 27 ± 2 nm for the hematite layers and 6 ± 1 nm for the Au layers grown at lower temperature (see SI). Representative high-angle XRR measurements for the Au/α-Fe_2O_3/oxide substrate heterostructures are shown in Figure 2a together with spectra for single α-Fe_2O_3 thin films grown on AO(0001) and STO(111) substrates, for comparison. The deposition of Au on top of the hematite layers results in a wide peak for low Au growth temperature masking the diffraction peak related to the epitaxial α-Fe_2O_3 layer, especially for the layer grown on STO(111). Increasing the growth temperature of noble metal, the Au peak becomes narrower and the

DOI: 10.1021/acs.jpcc.9b04768
J. Phys. Chem. C XXXX, XXX, XXX−XXX

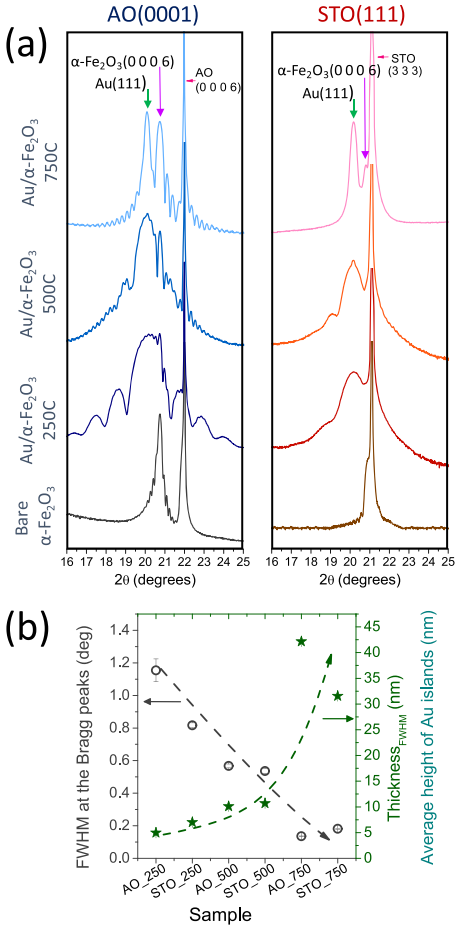

Figure 2. (a) High-angle θ–2θ scans for Au NPs prepared on α-Fe_2O_3(0001)/AO(0001) and α-Fe_2O_3(0001)/STO(111) oxide heterostructures varying the substrate temperature (250, 500, and 750 °C) for the growth of the Au nanostructured layers. GIXRD measurements for bare α-Fe_2O_3 thin films are also presented. Bragg peaks related to substrate, Au, and α-Fe_2O_3 are identified. A clear modification of the diffraction signal associated with the Au is observed due to its morphological features. (b) FWHM at the Au Bragg peaks and average height of Au islands obtained from the analysis of Bragg peaks of high-angle θ–2θ measurements.

diffraction peak related to hematite is more clearly distinguished on both types of substrates. The high-angle XRR spectra also reveal the presence of single-phase epitaxial α-Fe_2O_3 with (0001) orientation, as we identified for similar α-Fe_2O_3 systems in ref[30] and epitaxial Au with an orientation (111) irrespective of the chosen substrate. Besides, it should be noted that Kiessig fringes around thin-film Bragg peaks can be observed, more notably for sample grown on AO(0001) as we have recognized in single hematite layers grown on AO(0001) substrate.[30] Here, other fringes periodicity related to the nanostructured Au layer is recognized, indicating the occurrence of high-quality and smooth surfaces and abrupt hematite–substrate and Au–hematite interfaces. An in-depth analysis from high-angle XRR data helps to complete the morphological results provided by SEM, offering additional information about the thickness of Au nanostructured layer and of the average height of Au islands. From a careful analysis of the full width at half-maximum (FWHM) at the Au diffraction peaks, we have estimated the average height of Au islands to vary from around 5 to 40 nm, which increases as the substrate temperature increases during the Au growth, as presented in Figure 2b.

The morphological and structural features of the final Au islands can be attributed to diverse factors such as the processing conditions,[19,25,40–42] and the evolution of the nanostructuration can be ascribed to a convolution of several effects: the difference in the thermal expansion coefficient between the Au (14.2×10^{-6} K^{-1} at 20 °C) and the hematite film (8×10^{-6} K^{-1} at 20 °C),[43] the activation energy under the specific growth conditions in oxygen atmosphere, diffusion effects, Ostwald's ripening, and/or possible sublimation processes, of which none of them can be discarded.

These results indicate that the most significant morphological parameters such as the average size and height of Au islands and the hematite covered surface are dependent on the substrate temperature for the Au growth and not significantly on the type of oxide substrate employed in this work. However, the epitaxial quality and abruptness of the interfaces keep influenced by the selected substrate, which are enhanced for samples prepared on AO(0001) substrates.

Out-of-plane lattice parameters have been calculated from the measured peak position with respect to the substrate obtaining $c_{H/AO}$ = 13.72 (6) Å–c_{AO} and $c_{H/STO}$ = 13.72 (6) Å–$2c_{STO}$ for hematite layers grown on AO(0001) and STO(111), respectively, and $c_{Au/H/AO}$ = 7.05 (3) Å–1/2 $c_{H/AO}$ and $c_{Au/H/STO}$ = 7.05 (4) Å–1/2$c_{H/STO}$ for Au layers prepared on α-Fe_2O_3(0001)/AO(0001) and α-Fe_2O_3(0001)/STO(111), respectively, as resumed in Table 2. These calculated lattice parameters are consistent with those values obtained from the analysis of nonspecular out-of-plane scans (not shown) and the

Table 2. Domain Size and Lattice Parameters Obtained from the GIXRD Characterization for Au NPs Prepared on α-Fe_2O_3(0001)/AO(0001) and α-Fe_2O_3(0001)/STO(111) Oxide Heterostructures Varying the Substrate Temperature (250, 500, and 750 °C) during the Growth of the Au Nanostructured Layer

samples		domain size (Å)	out-plane lattice parameter (Å)	in-plane lattice parameter (Å)
Bare α-Fe_2O_3 on AO(0001)		400 (5)	13.72 (6)	5.08 (4)
AO_250	Au	150 (5)	7.05 (3)	2.90 (2)
	α-Fe_2O_3	370 (18)	13.72 (3)	5.08 (1)
AO_500	Au	170 (5)	7.05 (3)	2.90 (3)
	α-Fe_2O_3	380 (12)	13.70 (6)	5.08 (1)
AO_750	Au	200 (6)	7.05 (2)	2.90 (1)
	α-Fe_2O_3	350 (16)	13.69 (2)	5.08 (1)
Bare α-Fe_2O_3 on STO(111)		250 (4)	13.72 (6)	5.08 (4)
STO_250	Au	170 (5)	7.04 (2)	2.89 (2)
	α-Fe_2O_3	250 (1)	13.72 (3)	5.07 (1)
STO_500	Au	190 (10)	7.05 (4)	2.90 (1)
	α-Fe_2O_3	250 (11)	13.72 (3)	5.07 (1)
STO_750	Au	230 (9)	7.05 (3)	2.90 (1)
	α-Fe_2O_3	250 (9)	13.70 (6)	5.08 (2)

[a]Values obtained for single α-Fe_2O_3 films, reported in ref 30, are included for comparison.

DOI: 10.1021/acs.jpcc.9b04768
J. Phys. Chem. C XXXX, XXX, XXX–XXX

values estimated in single α-Fe_2O_3 layers, as previously reported.[30]

Figure 3 shows representative reciprocal space maps (RSM) for Au NPs grown on α-Fe_2O_3(0001)/AO(0001) and α-Fe_2O_3(0001)/STO(111) oxide heterostructures. Both Au and hematite layers grow incommensurate as is envisaged, based on the noncoincidence of the in-plane diffraction maxima from both type of layers and the corresponding substrate. An incommensurate growth was already established for single α-Fe_2O_3 fabricated on both oxide substrates.[30] Here, some features related to the nanostructuration of Au layer can be noted on RSM measurements. The surface signal revealed for Au diffraction peaks, which is characterized by the diffuse signal present between Bragg peaks, is reduced as the Au growth temperature increases. This result is related to a more isolated character of Au islands, promoting a larger roughness of the Au layer surfaces. Besides, differences in the shape of Au Bragg peaks are avowed. Narrower peaks in the out-of-plane direction of reciprocal space are obtained for the bilayers grown on both substrates as the substrate temperature increases in the Au growth, which is related to higher Au islands in excellent accordance with the high-angle XRR results.

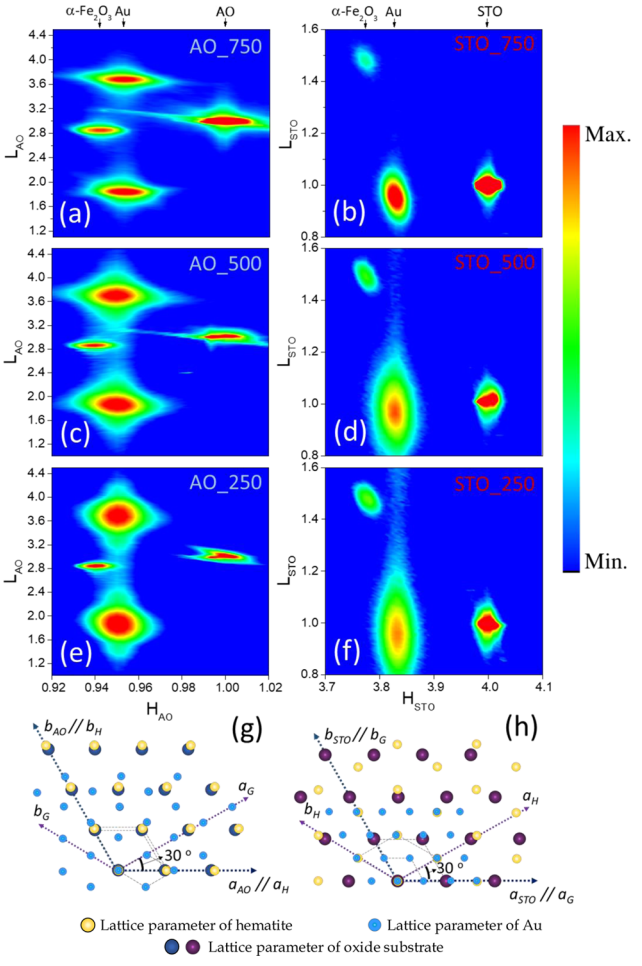

Figure 3. (a–f) LH reciprocal space maps (RSM) for Au NPs grown on α-Fe_2O_3(0001)/AO(0001) and α-Fe_2O_3(0001)/STO(111) oxide heterostructures varying the growth substrate temperature (250, 500, and 750 °C) of the Au nanostructured layer. From the in-plane diffraction measurements, we identify a noncoincidence of Au, α-Fe_2O_3, and substrates peaks, evidencing an incommensurate epitaxial growth. The color scale corresponds to the signal intensity. (g, h) Representative scheme in real space of the lattice coupling for the Au/α-Fe_2O_3 system on both substrates. $_{ax}$ and b_x represent the in-plane lattice parameters of x: S (substrate), H (hematite), and G (gold).

From the RSM measurements, the coupling behavior between the Au lattice, the hematite lattice, and the corresponding substrate lattice is achieved. In a previous study,[30] we determined an incommensurate coupling in the α-Fe_2O_3(0001)/STO(111) and the α-Fe_2O_3(0001)/AO(0001) systems, in which in-plane crystallographic axes of hematite lattice remain parallel to those of the AO(0001) substrate while a rotation of 30° occurs between hematite and STO(111) substrate lattices. In the present case, a similar behavior is obtained, concluding that the lattice coupling of the α-Fe_2O_3 on both substrates remains unaltered after the Au growth. With respect to the Au nanostructured layer grown on hematite one, its in-plane crystallographic axes are rotated 30° with respect to the hematite ones irrespectively of the substrate. Thus, a rotation of 30° is found between the Au and AO(0001) lattices, whereas in-plane crystallographic axes of Au lattice are collinear with those of the STO(111) substrate. Representative lattice models in real space of growth for Au/α-Fe_2O_3/oxide substrate systems are depicted in Figure 3g,h. The lattice orientation relationships between the layers and the substrates are revealed to be: Au/α-Fe_2O_3/AO(0001): (111) $[110]_{Au}$ ‖ (0001) $[100]_H$ ‖ (0001) $[100]_{AO}$ and Au/α-Fe_2O_3/STO(111): (111) $[110]_{Au}$ ‖ (0001) $[100]_H$ ‖(111) $[110]_{STO}$.

The obtained in-plane real space lattice parameters of the Au/α-Fe_2O_3 heterostructures based on the positions at several diffraction peaks in reciprocal space are $a_H = b_H \sim 5.08$ (4) Å for hematite and $a_{Au} = b_{Au} \sim 2.90$ (2) Å for Au lattice, as Table 2 presents. It should be noted that epitaxial hematite thin films grown on both substrates present the same lattice parameters before and after the deposition of Au layers, suggesting the stability of hematite lattice during the growth process of Au. For all layers, the obtained lattice parameters match, within the error, those of the bulk structure, revealing a stress-free character.

The in-plane domain size of the grown films was also calculated to be around 350 and 250 Å for the epitaxial hematite in the complex system deposited on AO(0001) and STO(111) substrate, respectively. Similar values were reported for bare hematite layers grown on the same substrates[30] without the *posteriori* evaporation of Au islands, reaffirming the nonalteration of hematite with the growth process of Au layer. As explained in ref,[30] the larger domain size of the α-Fe_2O_3(0001)/AO(0001) film is related to the more favorable growth based on the isostructural character between compounds. With respect to the nanostructured Au thin films, the in-plane domain size is estimated to be between 150 and 230 Å, following a trend with the Au growth conditions: higher the Au growth temperature, larger the domain sizes of epitaxial Au. Table 2 shows lattice parameters and the average values of the domains size obtained for each epitaxial layer on both oxide substrates employed.

Although from a structural point of view the hematite layers remain unaltered after Au deposition, important modifications on the iron and oxygen stoichiometry could happen as a way to favor the incommensurate Au-α-Fe_2O_3 coupling. To discharge possible iron oxide phase changes induced during the Au nanostructured adlayer growth, a series of XAS measurements

DOI: 10.1021/acs.jpcc.9b04768
J. Phys. Chem. C XXXX, XXX, XXX−XXX

have been carried out. From X-ray absorption near-edge structure (XANES) measurements achieved at the Fe K-edge, we corroborate the nature of hematite layers as single iron oxide phase for all samples after the deposition of Au islands. Indistinctly of oxide substrate selected and substrate temperature for the Au growth, the XANES spectra features follow those obtained for bare hematite layers[30] and for powder hematite reference, as Figure 4a shows. Fitting the XANES

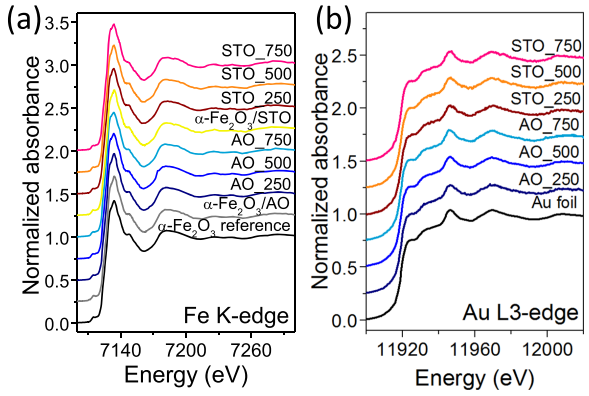

Figure 4. XANES spectra at the (a) Fe K-edge energy and (b) Au L_3-edge energy of Au(111)/α-Fe_2O_3(0001)/AO(0001) and Au(111)/α-Fe_2O_3(0001)/STO(111) systems varying the substrate temperature (250, 500, and 750 °C) for the growth of the Au nanostructured layer. XANES spectra of α-Fe_2O_3 powder reference, bare α-Fe_2O_3 films (α-Fe_2O_3/AO(0001) and α-Fe_2O_3/STO(111)),[30] and Au foil reference are presented for comparison in each case.

spectra with a linear combination of different iron oxide reference compounds (FeO, Fe_3O_4, α-Fe_2O_3, and γ-Fe_2O_3 references)[44] confirms a valence 3+ for Fe corresponding to a 100% stoichiometric hematite phase for all Au(111)/α-Fe_2O_3(0001)/AO(0001) and Au(111)/α-Fe_2O_3(0001)/STO-(111) heterostructures, independently of the Au growth temperature reached in this work.

For the Au islands layers, the XANES profile follows that of Au foil and no differences are noted irrespective of the substrate and/or the Au growth temperature, as shown in Figure 4b. Similar results are obtained from the X-ray photoelectron spectroscopy (XPS) measurements (see the SI) on the Au 4f core level. The spin−orbit splitting of 3.7 eV and the intensity relationship between both peaks ($4f_{5/2}$ to $4f_{7/2}$) corresponds to that of pure Au being identical for all samples. Moreover, we detect signal corresponding to the α-Fe_2O_3 surface on samples with the Au prepared at higher temperature corroborating the more isolated character of Au NSs. The combination of XANES and XPS demonstrates the absence of mixed Fe−Au phases present on the surface and buried interfaces.

The short-range ordering of cations around the Fe and Au and the neighbor bond lengths in nanostructured Au/α-Fe_2O_3/oxide substrate systems were analyzed by extended X-ray absorption fine structure (EXAFS) technique. Figure 5a displays the modulus of the Fourier transform (FT) of the EXAFS signal at the Au L_3-edge. The FT is performed in the $k^2\chi(k)$ weighted EXAFS signal between 2.8 and 8.0 $Å^{-1}$. Experimental EXAFS results are fitted in R-space in the range 1.6−3.3 Å (first neighbors) using the FEFFIT code.[45] The fitting was performed fixing the shift at the edge energy E_0, which was previously calculated from Au foil. Therefore, the

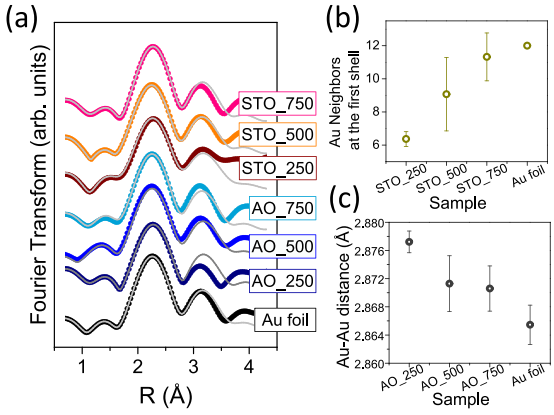

Figure 5. (a) FT modulus of the EXAFS signal (lines with symbols) and best-fitting simulations (continuous lines) at the Au L_3-edge of all samples and Au foil reference, (b) first neighbors Au−Au number for Au(111)/α-Fe_2O_3(0001)/STO(111) system, and (c) Au−Au distance at the first shell number for Au(111)/α-Fe_2O_3(0001)/AO(0001) system obtained from experimental EXAFS results measured at RT for heterostructures prepared varying the substrate temperature (250, 500, and 750 °C) for the growth of the Au nanostructured layer. Results of Au−Au first shell number and distance are representative of the two substrate employed and compared to the values obtained for the Au foil reference.

amplitude reduction factor S_0^2, the interatomic distance R, and the Debye−Waller (DW) factors σ^2 for the first shell are used as free parameters for the fitting.

With respect to the DW factors (not shown) obtained for the samples analyzed at the Au L_3-edge, these are of same order for all samples and any tendency is observed as a function of the chosen substrate and/or the substrate temperature during the Au growth. However, a variation of the coordination number (calculated from the amplitude factor S_0^2) and the first neighbors distance is found, as Figure 5b,c shows representatively for the heterostructures prepared on STO(111) and AO(0001) substrate, respectively. An increase of the Au neighbors number and a shortening of the Au−Au bond length at the first coordination shell are obtained as the substrate temperature is increased. Lower Au-neighbor number and larger Au−Au bond lengths are obtained for all samples compared to bulk Au. These EXAFS results agree with XRD measurements presented in the SI (Figure S3), indicating a larger crystalline order of the Au layer grown at higher temperatures.

For the Au/α-Fe_2O_3/oxide substrate systems at the Fe K-edge, a similar EXAFS study was carried out (not shown), revealing the absence of an additional short order with respect to single hematite films grown on AO(0001) and STO(111) substrate,[30] in accordance with XRD and XANES results.

Optical Characterization: Surface Plasmon Activity. The plasmonic response of Au NPs grown on α-Fe_2O_3(0001)/AO(0001) and α-Fe_2O_3(0001)/STO(111) oxide heterostructures was examined by the extinction spectra, and the results are displayed in Figure 6, representing a convolution of absorption and scattering processes. All systems present an extinction maximum associated with the localized surface plasmon resonance (LSPR) of Au islands arranged on the α-Fe_2O_3 surface. This LSPR band is located between 600 and 900 nm, varying its position depending on the morphological features of the NSs based on the different substrate temperature during the Au growth process.

DOI: 10.1021/acs.jpcc.9b04768
J. Phys. Chem. C XXXX, XXX, XXX−XXX

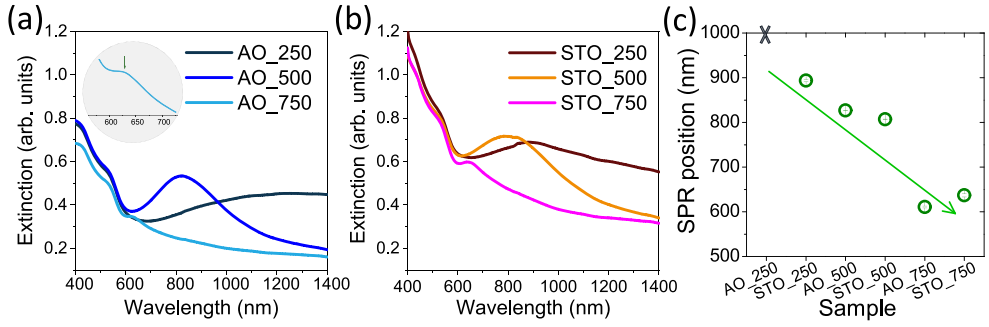

Figure 6. Extinction spectra for Au(111) islands prepared on (a) α-Fe_2O_3(0001)/AO(0001) and (b) α- Fe_2O_3(0001)/STO(111) oxide heterostructures as a function of the Au growth temperature (250, 500, and 750 °C). (c) Position at the LSPR maxima for the several samples prepared in this work. Sample AO_250 is marked with a cross in (c) indicating the absence of an extinction maximum. The inset in (a) shows a zoom of the LSPR region for the sampleAO_750 for a better identification.

Samples prepared at 500 and 750 °C of Au growth temperature show average size of Au NSs around 30 and 50 nm, respectively, as shown in Figure 1g, which exhibits the extinction spectra with an LSPR signal that is practically due to absorption effects. However, for the Au nanostructures prepared at 250 °C, the lateral average size is larger than 80 nm, with an LSPR shift toward larger wavelengths and a broader and asymmetric peak that is attributed to larger scattering effects, which has to be considered for several applications as, for example, for biological applications or for cell imaging and photochemical studies.[46,47]

Independently of the oxide substrate, the LSPR related to the Au NSs for all complex heterostructures exhibits a blue shift and a narrowing of band as Au substrate temperature increases, as can be clearly seen in Figure 6, which can be attributed to variations in the shape and interparticle distance of Au islands.[48,49] Moreover, in all instances, an additional shift of the LSPR bands is shown toward larger wavelength with respect to single Au islands. These changes in the position of the resonance band are due to the hematite layer rounding partially the Au islands, prompting an increase of the dielectric constant of their surrounding medium and with that the wavelength shift of plasmon resonance.[49,50]

For the case of samples with the Au layer prepared at high temperature (750 °C), the LSPR band is more similar to that expected for isolated Au NPs with a large distance between particles, a more rounded character, and a more homogeneous particle distribution. For the samples where the Au NSs are prepared at a substrate temperature of 500 °C, we find a shorter interparticle distance and a wider distribution of Au particle size, shifting the LSPR position toward larger wavelengths and widening its LSPR band.[49,50] This effect is accented for the Au/α-Fe_2O_3/STO(111) system grown at 250 °C with a more continuous Au layer. For the specific case of Au/α-Fe_2O_3/AO(0001) prepared at a temperature of 250 °C during the Au growth, we identify a plateau extended up to the near-infrared region in the extinction spectrum, instead of a well-defined maximum characteristic of localized surface plasmons (LSPs). This feature has already been reported for single nanostructured layers in the proximity of a continuous film and explained through the interaction between LSPs and extended SPs (expected in metallic thin films under specific conditions),[19,25,51] raising the plasmonic applications of these complex systems.

On the other hand, intensity variations of the LSPR are noted depending on the substrate temperature in the growth of Au islands, which might associate with parameters such as the Au islands size and/or the average dielectric constant in each system prepared.[48] Even, a sublimation process cannot be discarded at higher temperatures (750 °C), as commented above, diminishing markedly the intensity of the resonance band.

Finally, it should be noted that for all optical spectra of Au/α-Fe_2O_3/oxide substrate heterostructures, the LSPR bands of Au NPs appear superimposed on the optical signal related to the electronic transitions of α-Fe_2O_3 layer.[52,53] However, in the wavelength range where SPs of Au islands are excited, the absorption signal related to iron oxide is low and can be considered negligible.

4. CONCLUSIONS

We have shown the way to grow epitaxial incommensurate nanostructured Au(111) on α-Fe_2O_3(0001)/α-Al_2O_3(0001) and α-Fe_2O_3(0001)/$SrTiO_3$(111) oxide heterostructures. The Au nanostructured layer is obtained by a just one-step process controlling the substrate temperature during the Au growth, being the parameter that allows to tune the morphological and structural features of the Au nanostructures. After the Au growth, the stability of single-phase and single-oriented α-Fe_2O_3(0001) layers is confirmed, finding the same structural characteristics that prior to the deposition of Au nanoparticles. The coupling of the Au(111) islands lattice with the α-Fe_2O_3(0001) lattice is mediated by a rotation of 30° between their crystallographic axes. The Au(111) and $SrTiO_3$(111) lattices are hence collinear, while a rotation of 30° happens respect to the α-Al_2O_3(0001) lattice. The increase of the Au growth temperature leads to a larger crystallographic domain size, a larger crystalline order, a larger interparticle distance, and a more rounded character for Au islands. In addition, complex bilayers exhibit plasmonic activity. Controlling the substrate temperature in the Au growth, a tailorable response of the localized surface plasmons related to Au nanoparticles is mediated through the morphological characteristics of Au islands and the proximity effect of the hematite layer. This processing route allows obtaining ensembles of plasmonic islands on oxide surface with an epitaxial character, allowing the combination of multiple functions of these hybrid nanomaterials and their increasing highly value for several applications.

DOI: 10.1021/acs.jpcc.9b04768
J. Phys. Chem. C XXXX, XXX, XXX−XXX

■ ASSOCIATED CONTENT

Supporting Information

The Supporting Information is available free of charge on the ACS Publications website at DOI: 10.1021/acs.jpcc.9b04768.

Reflection high-energy electron diffraction patterns during the deposition of Au/α-Fe_2O_3 heterostructures prepared on different substrates; thin-film thickness calculation from low-angle X-ray reflectivity measurements; crystallinity analysis from X-ray diffraction measurements as a function of the substrate employed and the evaporation temperature for the Au growth; and X-ray photoelectron spectroscopy measurements on the Au 4f core level of Au(111)/α-Fe_2O_3(0001)/oxide substrate systems (PDF)

■ AUTHOR INFORMATION

Corresponding Author

*E-mail: aida.serrano@esrf.fr.

ORCID

Aida Serrano: 0000-0002-6162-0014

Author Contributions

All authors have given approval to the final version of the manuscript.

Notes

The authors declare no competing financial interest.

■ ACKNOWLEDGMENTS

This work was supported by the Ministerio Español de Ciencia, Innovación y Universidades (MCIU), and the Consejo Superior de Investigaciones Cientificas (CSIC) through the project PIE-2010-OE-013-200014. J.L.-S. and E.E. acknowledge the FPI fellowship and the Torres Quevedo contract (ref: PTQ-14-07289). The ESRF, MCIU, and CSIC are acknowledged for the provision of synchrotron radiation facilities. The authors thank Dr M.A. García for the useful discussion about the plasmonic results and Carlos Beltrán for technical support during the experiments at the BM25 beamline at The ESRF.

■ REFERENCES

(1) Wang, L.; Wang, L.; Hu, H.; Truong, N.; Zhang, Y.; Schmuki, P.; Bi, Y. Plasmon-Induced Hole-Depletion Layer on Hematite Nanoflake Photoanodes for Highly Efficient Solar Water Splitting. *Nano Energy* **2017**, *35*, 171−178.

(2) Gao, H.; Liu, C.; Jeong, H. E.; Yang, P. Plasmon-Enhanced Photocatalytic Activity of Iron Oxide on Gold Nanopillars. *ACS Nano* **2012**, *6*, 234−240.

(3) Serrano, A.; Rodríguez de La Fuente, O.; García-Hernández, M.; Campo, G.; De Julián Fernández, C.; Fernández, J. F.; García, M. A. Tailoring Nanostructured Surfaces with Plasmonic/magnetic Multifunctional Response. *Appl. Phys. Lett.* **2018**, *113*, No. 10908.

(4) Ovejero, J. G.; Morales, I.; de la Presa, P.; Mille, N.; Carrey, J.; Garcia, M. A.; Hernando, A.; Herrasti, P. Hybrid Nanoparticles for Magnetic and Plasmonic Hyperthermia. *Phys. Chem. Chem. Phys.* **2018**, *20*, 24065−24073.

(5) Hsu, C. L.; Jhang, B. Y.; Kao, C.; Hsueh, T. J. UV-Illumination and Au-Nanoparticles Enhanced Gas Sensing of P-Type Na-Doped ZnO Nanowires Operating at Room Temperature. *Sens. Actuators, B* **2018**, *274*, 565−574.

(6) Zheng, W.; Chiamori, H. C.; Liu, G. L.; Lin, L.; Chen, F. F. Nanofabricated Plasmonic Nano-Bio Hybrid Structures in Biomedical Detection. *Nanotechnol. Rev.* **2012**, *1*, 213−233.

(7) Kim, S. M.; Lee, S. W.; Moon, S. Y.; Park, J. Y. The Effect of Hot Electrons and Surface Plasmons on Heterogeneous Catalysis. *J. Phys. Condens. Matter* **2016**, *28*, No. 254002.

(8) Lee, S. W.; Hong, J. W.; Lee, H.; Wi, D. H.; Kim, S. M.; Han, S. W.; Park, J. Y. The Surface Plasmon-Induced Hot Carrier Effect on the Catalytic Activity of CO Oxidation on a Cu_2O/hexoctahedral Au Inverse Catalyst. *Nanoscale* **2018**, *10*, 10835−10843.

(9) Zhang, J.; Liu, X.; Wang, L.; Yang, T.; Guo, X.; Wu, S.; Wang, S.; Zhang, S. Au-Functionalized Hematite Hybrid Nanospindles: General Synthesis, Gas Sensing and Catalytic Properties. *J. Phys. Chem. C* **2011**, *115*, 5352−5357.

(10) Gatel, C.; Snoeck, E. Epitaxial Growth of Au and Pt on Fe_3O_4(1 1 1) Surface. *Surf. Sci.* **2007**, *601*, 1031−1039.

(11) Muñoz-Noval, A.; Rubio-Zuazo, J.; Salas-Colera, E.; Serrano, A.; Rubio-Marcos, F.; Castro, G. R. Large Coincidence Lattice on Au/Fe_3O_4 incommensurate Structure for Spintronic Applications. *Appl. Surf. Sci.* **2015**, *355*, 698−701.

(12) Freund, S. S.; Fritz, H. J. Ultrathin Oxide Films on Metal Supports: Structure-Reactivity Relations. *Annu. Rev. Phys. Chem.* **2012**, *63*, 619−633.

(13) Zeng, L.; Li, K.; Wang, H.; Yu, H.; Zhu, X.; Wei, Y.; Ning, P.; Shi, C.; Luo, Y. CO Oxidation on Au/α-Fe_2O_3-Hollow Catalysts: General Synthesis and Structural Dependence. *J. Phys. Chem. C* **2017**, *121*, 12696−12710.

(14) Shen, S.; Lindley, S. A.; Chen, X.; Zhang, J. Z. Hematite Heterostructures for Photoelectrochemical Water Splitting: Rational Materials Design and Charge Carrier Dynamics. *Energy Environ. Sci.* **2016**, *9*, 2744−2775.

(15) Schultz, A. M.; Salvador, P. A.; Rohrer, G. S. Enhanced Photochemical Activity of α-Fe_2O_3 Films Supported on $SrTiO_3$ Substrates under Visible Light Illumination. *Chem. Commun.* **2012**, *48*, 2012−2014.

(16) Tuboltsev, V.; Savin, A.; Pirojenko, A.; Räisänen, J. Magnetism in Nanocrystalline Gold. *ACS Nano* **2013**, *7*, 6691−6699.

(17) Wang, L.; Zhu, Y.; Wang, J. Q.; Liu, F.; Huang, J.; Meng, X.; Basset, J. M.; Han, Y.; Xiao, F. S. Two-Dimensional Gold Nanostructures with High Activity for Selective Oxidation of Carbon-Hydrogen Bonds. *Nat. Commun.* **2015**, *6*, No. 8828.

(18) Madzharova, F.; Heiner, Z.; Simke, J.; Selve, S.; Kneipp, J. Gold Nanostructures for Plasmonic Enhancement of Hyper-Raman Scattering. *J. Phys. Chem. C* **2018**, *122*, 2931−2940.

(19) Serrano, A.; Rodri′guez de la Fuente, O.; Garci′a, M. A. Extended and Localized Surface Plasmons in Annealed Au Films on Glass Substrates. *J. Appl. Phys.* **2010**, *108*, No. 74303.

(20) Pastoriza-Santos, I.; Kinnear, C.; Pérez-Juste, J.; Mulvaney, P.; Liz-Marzán, L. M. Plasmonic Polymer Nanocomposites. *Nat. Rev. Mater.* **2018**, *3*, 375−391.

(21) Sai-Anand, G.; Philips, M. F.; Lee, K.-P.; Kang, S.-W.; Gopalan, A. I. Facile Electrodeposition of Flower Like Gold Nanostructures on a Conducting Polymer Support. *J. Nanosci. Nanotechnol.* **2014**, *14*, 3256−3261.

(22) Gopalan, S. A.; Gopalan, A. I.; Vinu, A.; Lee, K. P.; Kang, S. W. A New Optical-Electrical Integrated Buffer Layer Design Based on Gold Nanoparticles Tethered Thiol Containing Sulfonated Polyaniline towards Enhancement of Solar Cell Performance. *Sol. Energy Mater. Sol. Cells* **2018**, *174*, 112−123.

(23) Thompson, C. V. Solid-State Dewetting of Thin Films. *Annu. Rev. Mater. Res.* **2012**, *42*, 399−434.

(24) Leroy, F.; Borowik, Ł.; Cheynis, F.; Almadori, Y.; Curiotto, S.; Trautmann, M.; Barbe, J. C.; Müller, P. How to Control Solid State Dewetting: A Short Review. *Surf. Sci. Rep.* **2016**, *71*, 391−409.

(25) Serrano, A.; Llorca-Hernando, O.; Del Campo, A.; Rubio-Marcos, F.; Rodríguez de La Fuente, O.; Fernández, J. F.; García, M. A. Ag-AgO Nanostructures on Glass Substrates by Solid-State Dewetting: From Extended to Localized Surface Plasmons. *J. Appl. Phys.* **2018**, *124*, No. 133103.

(26) Hu, X.; Cahill, D. G.; Averback, R. S. Nanoscale Pattern Formation in Pt Thin Films due to Ion-Beam-Induced Dewetting. *Appl. Phys. Lett.* **2000**, *76*, No. 3215.

(27) Krasheninnikov, A. V.; Nordlund, K. Ion and Electron Irradiation-Induced Effects in Nanostructured Materials. *J. Appl. Phys.* **2010**, *107*, No. 071301.
(28) Altomare, M.; Nguyen, N. T.; Schmuki, P. Templated Dewetting: Designing Entirely Self-Organized Platforms for Photocatalysis. *Chem. Sci.* **2016**, *7*, 6865−6886.
(29) Lachebi, I.; Fedala, A.; Djenizian, T.; Hadjersi, T.; Kechouane, M. Morphological and Optical Properties of Aluminum Nanoparticles Deposited by Thermal Evaporation on Heated Substrates. *Surf. Coatings Technol.* **2018**, *343*, 160−165.
(30) Serrano, A.; Rubio-Zuazo, J.; López-Sánchez, J.; Arnay, I.; Salas-Colera, E.; Castro, G. R. Stabilization of Epitaxial α-Fe_2O_3 Thin Films Grown by Pulsed Laser Deposition on Oxide Substrates. *J. Phys. Chem. C* **2018**, *122*, 16042−16047.
(31) Rubio-Zuazo, J.; Ferrer, P.; López, A.; Gutiérrez-león, A.; Silva, I.; Castro, G. R. Nuclear Instruments and Methods in Physics Research A The Multipurpose X-Ray Diffraction End-Station of the BM25B-SpLine Synchrotron Beamline at the ESRF. *Nucl. Instrum. Methods Phys. Res., Sect. A* **2013**, *716*, 23−28.
(32) Ravel, B.; Newville, M. ATHENA, ARTEMIS, HEPHAESTUS: Data Analysis for X-Ray Absorption Spectroscopy Using IFEFFIT. *J. Synchrotron Radiat.* **2005**, *12*, 537−541.
(33) Farzinpour, P.; Sundar, A.; Gilroy, K. D.; Eskin, Z. E.; Hughes, R. A.; Neretina, S. Altering the Dewetting Characteristics of Ultrathin Gold and Silver Films Using a Sacrificial Antimony Layer. *Nanotechnology* **2012**, *23*, No. 495604.
(34) Seguini, G.; Llamoja Curi, J.; Spiga, S.; Tallarida, G.; Wiemer, C.; Perego, M. Solid-State Dewetting of Ultra-Thin Au Films on SiO_2 and HfO_2. *Nanotechnology* **2014**, *25*, No. 495603.
(35) Bernardo-Gavito, R.; Serrano, A.; Garci′a, M. A.; Miranda, R.; Granados, D. Local Characterization of the Optical Properties of Annealed Au Films on Glass Substrates. *J. Appl. Phys.* **2013**, *114*, No. 164312.
(36) Lo Savio, R.; Repetto, L.; Batič, B. Š.; Firpo, G.; Valbusa, U. Local Nanostructuring of Gold Thin Films through Dewetting Induced by Ga^+ Irradiation. *Nucl. Instrum. Methods Phys. Res., Sect. B* **2015**, *354*, 129−133.
(37) Presland, A. E. B.; Price, G. L.; Trimm, D. L. Hillock Formation by Surface Diffusion on Thin Silver Films. *Surf. Sci.* **1972**, *29*, 424−434.
(38) Simrick, N. J.; Kilner, J. A.; Atkinson, A. Thermal Stability of Silver Thin Films on Zirconia Substrates. *Thin Solid Films* **2012**, *520*, 2855−2867.
(39) Sharma, S. K.; Spitz, J. Hillock Formation, Hole Growth and Agglomeration in Thin Silver Films. *Thin Solid Films* **1980**, *65*, 339−350.
(40) Sui, M.; Pandey, P.; Kunwar, S.; Li, M. Y.; Zhang, Q.; Lee, J. Evolution of Self-Assembled Ag Nanostructures on c-Plane Sapphire by the Systematic Control of Annealing Temperature. *Superlattices Microstruct.* **2016**, *100*, 1128−1142.
(41) Li, M. Y.; Zhang, Q.; Pandey, P.; Sui, M.; Kim, E. S.; Lee, J. From the Au Nano-Clusters to the Nanoparticles on 4H-SiC (0001). *Sci. Rep.* **2015**, *5*, No. 13954.
(42) Pandey, P.; Kunwar, S.; Sui, M.; Bastola, S.; Lee, J. Compositional Effect on the Fabrication of Ag_xPd_{1-X} Alloy Nanoparticles on c-Plane Sapphire at Distinctive Stages of the Solid-State-Dewetting of Bimetallic Thin Films. *RSC Adv.* **2017**, *7*, 55471−55481.
(43) Touloukian, Y. S.; Kirby, R. K.; Taylor, R. E.; Desai, P. D. *Thermal Expansion: Metallic Elements and Alloys (Thermophysical Properties of Matter, Vol. 12*; 1st ed.; IFI/Plenum, 1975.
(44) Rubio-Zuazo, J.; Chainani, A.; Taguchi, M.; Malterre, D.; Serrano, A.; Castro, G. R. Electronic Structure of FeO, γ-Fe_2O_3, and Fe_3O_4 Epitaxial Films Using High-Energy Spectroscopies. *Phys. Rev. B* **2018**, *97*, 1−9.
(45) Newville, M.; Ravel, B.; Haskel, D.; Rehra, J. J.; Stern, E. A.; Yacoby, Y. Analysis of Multiple-Scattering XAFS Data Using Theoretical Standards. *Phys. Rev. B: Condens. Matter* **1995**, *209*, 154−156.
(46) Liu, B. J.; Lin, K. Q.; Hu, S.; Wang, X.; Lei, Z. C.; Lin, H. X.; Ren, B. Extraction of Absorption and Scattering Contribution of Metallic Nanoparticles toward Rational Synthesis and Application. *Anal. Chem.* **2015**, *87*, 1058−1065.
(47) Jain, P. K.; Lee, K. S.; El-Sayed, I. H.; El-Sayed, M. A. Calculated Absorption and Scattering Properties of Gold Nanoparticles of Different Size, Shape, and Composition: Applications in Biological Imaging and Biomedicine. *J. Phys. Chem. B* **2006**, *110*, 7238−7248.
(48) Garcia, M. A. Surface Plasmons in Metallic Nanoparticles: Fundamentals and Applications. *J. Phys. D.: Appl. Phys.* **2011**, *44*, No. 283001.
(49) Serrano Rubio, A. *Modified Au-Based Nanomaterials Studied by Surface Plasmon Resonance Spectroscopy*; Springer Theses, 2015.
(50) Serrano, A.; Fernández, J. F.; Rodríguez de la Fuente, O.; García, M. A. A Novel Route to Obtain Metal and Oxide Nanoparticles Co-Existing on a Substrate. *Mater. Today Chem.* **2017**, *4*, 64−72.
(51) Cesario, J.; Gonzalez, M. U.; Cheylan, S.; Barnes, W. L.; Enoch, S.; Quidant, R. Coupling Localized and Extended Plasmons to Improve the Light Extraction through Metal Films. *Opt. Express* **2007**, *15*, 10533−10539.
(52) Cornell, R. M.; Schwertmann, U. *The Iron Oxides: Structure, Properties, Reactions, Occurrence and Uses*, 2nd ed.; Wiley-VCH Verlag GmbH & Co. KGaA: Weinheim, 2003.
(53) He, Y. P.; Miao, Y. M.; Li, C. R.; Wang, S. Q.; Cao, L.; Xie, S. S.; Yang, G. Z.; Zou, B. S.; Burda, C. Size and Structure Effect on Optical Transitions of Iron Oxide Nanocrystals. *Phys. Rev. B* **2005**, *71*, No. 125411.

DOI: 10.1021/acs.jpcc.9b04768
J. Phys. Chem. C XXXX, XXX, XXX−XXX